IOPscience iopscience.iop.org

Home Search Collections Journals About Contact us My IOPscience

Wavy interface morphologies in strained $Si_{1-x}Ge_x/Si$ multilayers on vicinal Si(111) substrates

This article has been downloaded from IOPscience. Please scroll down to see the full text article.

1998 J. Phys.: Condens. Matter 10 8643

(http://iopscience.iop.org/0953-8984/10/39/003)

View the table of contents for this issue, or go to the journal homepage for more

Download details:
IP Address: 171.66.16.210
The article was downloaded on 14/05/2010 at 17:24

Please note that terms and conditions apply.

J. Phys.: Condens. Matter **10** (1998) 8643–8652. Printed in the UK PII: S0953-8984(98)94566-0

Wavy interface morphologies in strained $Si_{1-x}Ge_x$/Si multilayers on vicinal Si(111) substrates

J H Li†, Y Yamaguchi‡, H Hashizume‡∥, N Usami§ and Y Shiraki§

† Institute of Physics and Centre for Condensed Matter Physics, Chinese Academy of Sciences, PO Box 603, Beijing 100080, People's Republic of China

‡ Materials and Structures Laboratory, Tokyo Institute of Technology, Nagatsuta, Midori, Yokohama 226-8503, Japan

§ Research Centre for Advanced Science and Technology, University of Tokyo, Komaba, Meguro, Tokyo 153-8904, Japan

Received 26 May 1998, in final form 16 July 1998

Abstract. We report grazing-angle x-ray scattering investigations of interface morphologies in strained $Si_{1-x}Ge_x$/Si multilayers grown on vicinal Si(111) substrates. Samples with different Ge fractions in the alloy layers show a common feature of wavy interfaces arising from the substrate miscut and step bunching. They differ, however, quite remarkably in the wavy period. Our analyses show that the stress-driven step redistribution should take the responsibility for such behaviours of the interfaces.

1. Introduction

The interface roughness in artificial multilayers has attracted much attention because of its significant effects on the physical properties of the structures. In semiconductor multilayers, the random scattering of charge carriers at rough interfaces not only affects the carrier mobility, but may also destroy coherent effects such as resonant tunnelling. The characterization and control of the interface roughness is thus an essential issue in multilayer technology. With the recent development of scattering theory for rough interfaces in multilayers, the grazing-angle x-ray scattering method has become a powerful non-destructive technique for probing buried interface structures with atomic resolution [1–4].

SiGe/Si heterostructures, with their potential applications in optoelectronics and high-speed electronics based on the mature Si technology, have been intensively studied in recent years. One of the key issues here concerns the growth of flat SiGe layers on Si substrates. Many works have evidenced that a strained SiGe layer is morphologically unstable against misfit strain [5–7]. This instability often causes a planar film to transform to a 3D island and/or a ridge-like morphology. The importance of understanding and controlling the growth morphology of SiGe layers lies in the requirement for smooth surface/interfaces in many device applications. On the other hand, the strain-driven transition of the film morphology is exploited in the self-assembled quantum dots [8]. Besides the experimental investigations, a great many efforts have been dedicated to theoretical descriptions of these growth phenomena [9–11]. In strain-relaxed SiGe layers, the surface is characterized by

∥ Corresponding author: H Hashizume, Materials and Structures Laboratory, Tokyo Institute of Technology, Nagatsuta, Midori, Yokohama 226-8503, Japan. Email: hhashizu@n.cc.titech.ac.jp.

0953-8984/98/398643+10$19.50 © 1998 IOP Publishing Ltd

the so-called crosshatch morphology associated with misfit dislocations [12]. Anisotropic properties and layer-to-layer correlations [13–15], as well as dynamical scaling behaviours [16], have been studied for the interfaces in the SiGe/Si multilayers grown on Si(001) substrates.

In this paper, we report grazing-angle x-ray scattering measurements of the interface structures in $Si_{1-x}Ge_x$/Si multilayers grown on vicinal Si(111) substrates. We found that the surface steps, originated from the substrate miscut, play a dominant role in the formation of the interface structure in the multilayers grown on it. For vicinal Si(001) samples, it is known that the surface steps are usually equally spaced. The effect of an external stress on the surface, e.g. growth of a strained layer on it, is to cause the steps to form bunches [17]. For a vicinal Si(111) sample, however, the surface steps are bunched prior to applying any stress on it due to surface reconstruction [18]. Our results show that in this case, the external stress produced by the growth of strained SiGe alloy layers induces a stress-driven step redistribution. A simple thermodynamic model has been put forward to account for this phenomenon.

2. Experiment

The samples investigated here have 10-period bilayers of 5 nm $Si_{1-x}Ge_x$/5 nm Si, grown by gas-source molecular beam epitaxy (MBE) on Si(111) substrates. A Si layer of 5 nm in thickness was first grown at 800 °C, and then the multilayer structure was deposited at 550 °C. The growth rates for both the Si and $Si_{1-x}Ge_x$ layers are 0.1 nm s^{-1}. Growth of the samples was terminated by Si layers. Further details of our gas-souce epitaxy technique are reported elsewhere [19, 20]. The substrate surfaces were miscut away from the (111) plane by $0.6 \pm 0.05°$ in the $[11\bar{2}]$ direction. The Ge contents of the $Si_{1-x}Ge_x$ alloy layers in our multilayers are 10% (sample 1) and 30% (sample 2). It is well known that the lattice constant of the relaxed $Si_{1-x}Ge_x$ alloy layer is $4.2x$% larger than that of Si. This means that pseudomorphic SiGe alloy layers with 30% Ge are subject to a three times higher in-plane compressive stress than those with 10% Ge.

X-ray experiments were performed using a Rigaku diffractometer with Cu $K\alpha_1$ radiation. A two-bounce Si(111) crystal with an asymmetric channel was used in the incident beam optic as a monochromator, giving x-rays of a divergence smaller than 75 arc s. The detector, located 30 cm away from the sample, consists of a 100 μm slit in the scattering plane and an NaI scintillation counter. Both the sample and the detector can be rotated independently with an accuracy better than 0.001 degrees.

The geometry of grazing-angle scattering in reciprocal space is schematically shown in figure 1(a). The two principal scans used in our measurements are indicated. The q_z scan (labelled 1) measures the specular reflectivity, and the q_x scan (labelled 2) around a superlattice Bragg reflection (represented by the black dot) measures the diffuse scattering arising from interface roughness. In our measurements, q_x scans were made in two azimuthal orientations of the sample as shown in figure 1(b). In azimuth A (B), the plane of scattering, defined by $\boldsymbol{k}_{in}$ and $\boldsymbol{k}_{out}$, is parallel (perpendicular) to the miscut direction of the substrate.

3. Results and discussion

Figure 2 shows the q_x scans through the third-order Bragg reflection of sample 1. The two curves (a) and (b) correspond to azimuths A and B, respectively. The results show that the scattering from the multilayer sample is highly anisotropic. In curve (a), we observe a

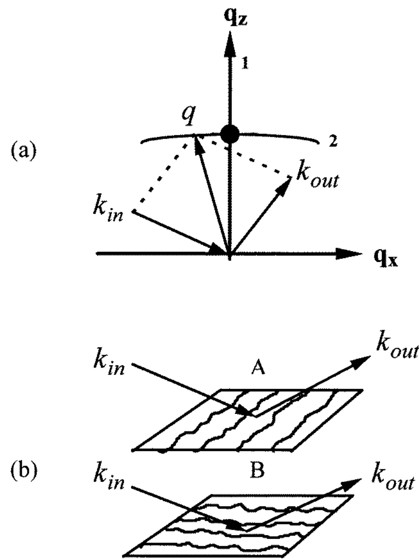

Figure 1. Schematic diagrams showing (a) scattering geometry in reciprocal space and (b) two sample configurations, A and B, with respect to the plane of x-ray scattering.

specular peak at $q_x = 0$ (labelled S) accompanied by a strong diffuse-scattering peak in the $-q_x$ region and a weak diffuse peak in the $+q_x$ region (indicated by arrows). The leftmost peak is the so-called Yoneda peak, which appears when the incidence angle of x-rays equals the critical angle for total external reflection [21]. The weak peak (labelled TS) seen between the Yoneda peak and the diffuse peak cannot be taken as a higher-order resonance of the diffuse peak since its separation from the nearby diffuse peak does not coincide with the spacing between the diffuse peak and the specular reflection. By performing a series of q_x scans in the vicinity of the third-order Bragg reflection, we found that in contrast to the diffuse peaks which appeared at fixed q_x positions in all scans, the q_x position of the peak TS was q_z dependent. Therefore, it must have a different origin which is not identified in this work.

Very differently, in curve (b), except for a Yoneda peak on the leftmost side, we observe only a narrow specular reflection sitting on a broad diffuse scattering. No distinct peaks are observed in either the $-q_x$ region or the $+q_x$ region. Similar anisotropic scattering features have been observed in other multilayers [13, 14]. These works suggest that the features observed in figure 2 can be attributed to anisotropic interface roughness. Along the miscut direction, the roughness is represented by a periodic waviness with a mean spatial wavelength $\langle L\rangle$, which gives rise to the diffuse peaks on both sides of the specular reflection in the q_x scan. The positions of the diffuse peaks in momentum space are determined by $|\delta q_x| = 2\pi/\langle L\rangle$, where δq_x is the separation of the diffuse peak from the specular peak. On the other hand, in the perpendicular direction (azimuth B), the roughness is random in nature, so that no distinct diffuse peak appears in the q_x scan. From figure 2(a), we determine a mean period of the interface waviness along the miscut direction in sample 1 to be $\langle L\rangle = 370 \pm 30$ nm.

The intensity distribution of the diffuse scattering on both sides of the specular reflection in azimuth A reflects the fine structure of the wavy interfaces. The relationship between the asymmetric diffuse intensity in the $-q_x$ and $+q_x$ regions and the property of the wavy

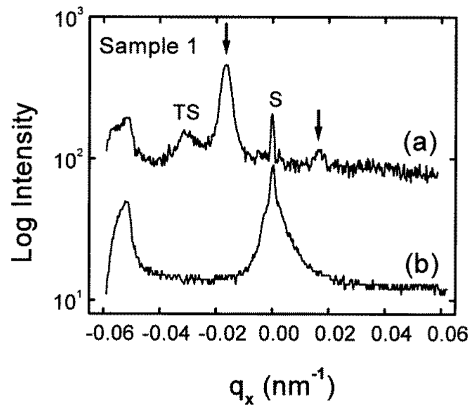

Figure 2. q_x scans on sample 1 through the third-order Bragg reflection. (a) For azimuth A; (b) for azimuth B.

interfaces was first discussed by Phang *et al* [14]. They showed that asymmetric diffuse intensities are an indication of different areas for the up-hill and the down-hill faces of wavy interfaces. The reflection geometry is not symmetric in such structures. If the diffuse intensity is symmetric in the $-q_x$ region and the $+q_x$ region, the up-hill and the down-hill faces must have similar areas. To understand this anisotropic interface feature, the property of the Si(111) surface has to be recalled. Many studies have shown that a vicinal Si(111) surface miscut along either the $\langle 1\bar{1}0\rangle$ or $\langle 11\bar{2}\rangle$ direction favours a two-phase structure below the 7×7 to 1×1 transition temperature ($T_c \sim 840\,°\mathrm{C}$) [18, 22, 23]. It consists of 7×7 reconstructed terraces with relatively large surface areas and densely stepped, unreconstructed regions with much smaller surface areas. The driving force for the formation of such a surface morphology is the lower energy of the 7×7 reconstructed surface, which makes a coalescence of the steps energetically favourable. Swartzentruber and co-workers report that the size of the step bunches (number of steps in a bunch) on vicinal Si(111) surfaces stays always around ten, regardless of the degree of the miscut angle [24].

If we correlate the interface waviness in our sample 1 with step bunching, the 0.6° miscut angle and the mean undulation wavelength $\langle L\rangle = 370$ nm should correspond to a mean step bunch height of about 3.8 nm. In other words, the bunch size is about 12 (a single step is 0.318 nm high). This value is very close to the reported bunch size on the vicinal Si(111) surfaces due to the 7×7 reconstruction. Further, in figure 2(a), the intensity of the diffuse-scattering peak in the $-q_x$ region is much higher than that in the $+q_x$ region. Such an extremely asymmetrical distribution of the diffuse intensity suggests that the face areas of the up- and down-hills of the interface waves in sample 1 differ significantly from each other. This is consistent with the surface structure of the vicinal Si(111) substrate. It is likely that the anisotropic interface feature in sample 1 is replicated from the substrate surface. In other words, the observed interface waviness, which consists of relatively wide terraces and narrow stepped facets, is caused by step bunching. This interface structure is schematically shown in figure 3(a). An atomic-force microscopy (AFM) image of the multilayer surface, shown in figure 4(a), does indeed show a wavy structure with a period of approximately 370 nm. It also shows terraces having a dominant surface area in each period. These are in agreement with the conclusions from our x-ray analysis. A unique feature in the AFM picture is the small islands (about 100 nm in size) seen on the terraces

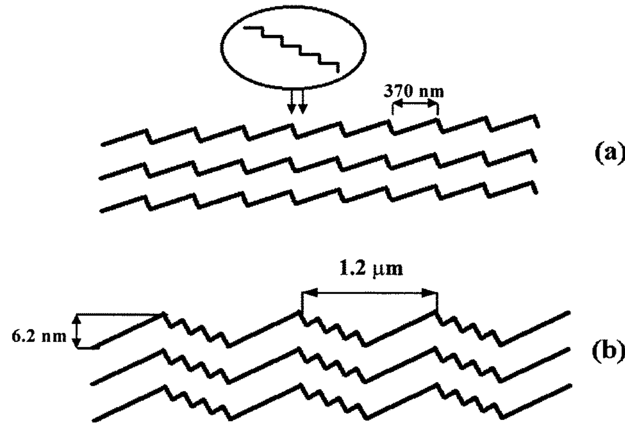

Figure 3. Schematics showing the step configurations for (a) sample 1, and (b) sample 2. The vertical scale has been enlarged for clarity. The number of steps shown do not correspond to the real one in our samples. The encircled diagram shows individual steps in the step bunch.

with three major orientations angled about 60°. These islands are similar to those observed on $Si_{1-x}Ge_x$ epilayers grown on Si(001) [6], and are likely to be formed by elastic strain relaxation. The three orientations of these elongated islands correspond to the threefold symmetry of our (111)-oriented sample.

Our explanation of the asymmetric diffuse peaks in terms of the distinct surface areas of the up-hills and down-hills implies that the larger peak and the smaller peak will appear at the interchanged positions in a reciprocal experiment where the directions of the x-ray beam are reversed, i.e. $\boldsymbol{k}_{in} \rightarrow -\boldsymbol{k}_{out}$ and $\boldsymbol{k}_{out} \rightarrow -\boldsymbol{k}_{in}$. This was indeed observed.

Figure 5 shows q_x scans through the third-order Bragg reflection of sample 2 with a Ge fraction of 30% in the SiGe layers. Here again the two curves (a) and (b) correspond to azimuths A and B, respectively. In curve (a), aside from the specular reflection at $q_x = 0$ (labelled S) and the Yoneda peak at the leftmost side, diffuse peaks of similar heights are seen on both sides of the specular reflection (indicated by vertical arrows). On the other hand, in curve (b), no diffuse maximum occurs on either side of the specular peak, although the latter is associated with a broad diffuse component as in figure 2(b). This result suggests that sample 2 has also an anisotropic interface morphology as sample 1, but significantly differs in two aspects from sample 1. First, the undulation wavelength along the miscut direction is much longer, about 1.2 ± 0.2 μm. Second, because the diffuse peaks on both sides of the specular reflection have similar intensities, the up- and down-hills of the interface undulation must have similar face areas in sample 2. This is to say that the growth of the epilayers in this sample does not follow the morphology of the substrate Si(111) surface, but forms a different structure. In figure 5(a), traces of a second diffuse-scattering component are seen, as indicated by horizontal arrows. Although not as evident as the first component discussed above, the positions of these secondary peaks exactly correspond to the scattering from the step bunches at the substrate surface. The overwhelming intensity of the first component suggests that the new interface structure has been formed at an early stage of the growth process, implying that it is of thermodynamic rather than kinetic origin. The appearance of the second component means that the step configuration has been conserved at the substrate surface. The change of the surface morphology occurred only in the epilayers. The surface topography of this sample observed by AFM, shown in figure 4(b), indicates indeed a mean

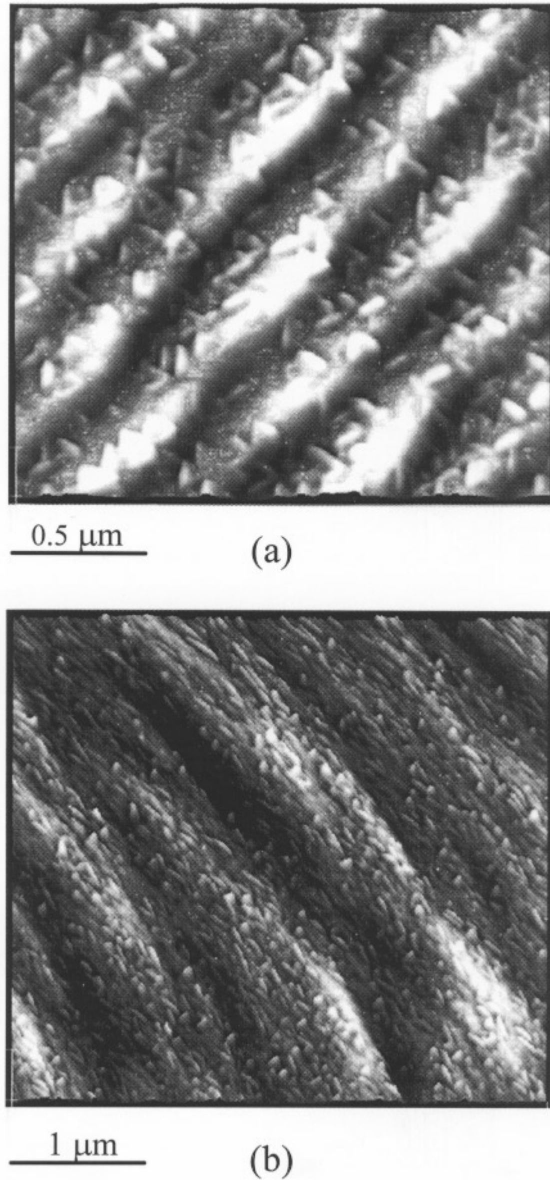

Figure 4. AFM images taken from the surface of (a) sample 1 and (b) sample 2. The miscut direction is parallel to the line connecting the top left and the bottom right corners in (a) and the line connecting the bottom left and the top right corners in (b).

wave period of about 1.2 μm along the miscut direction, in agreement with the x-ray result. However, the length of the surface wave is no longer as long as in sample 1, but ranges between 3 and 4 μm. Elongated islands, about 50–150 nm in size, covering the whole surface are also visible in figure 4(b).

The formation of the interface morphology in sample 2 with the larger undulation wavelength must be related to the higher Ge content in the alloy layers, since this sample

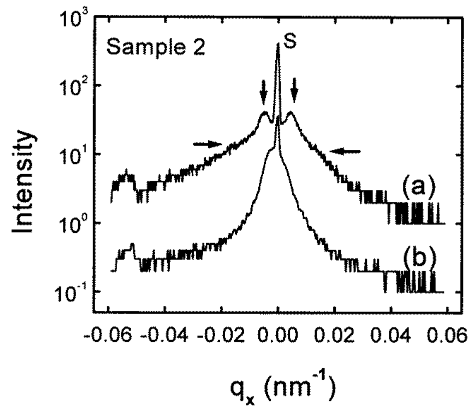

Figure 5. q_x scans on sample 2 through the third-order Bragg reflection. (a) For azimuth A and (b) for azimuth B.

is otherwise quite similar to sample 1. The high Ge content causes high stress in the alloy layers, and the stress can have significant effects on the morphology of the epilayer surface. 3D island growth [6] and formation of ripples [7] are well known. In our case, however, the island growth seems to play an unimportant role in the formation of the observed interface morphology, since the 3D island growth would result in isotropic roughness. Moreover, even if the nucleation of the islands is anisotropic because of the existence of steps at the substrate surface, the only 5 nm thick alloy layers would hardly erase the influence of the 3.8 nm high step bunches present at the substrate surface: they are probably replicated into the epilayers as in sample 1. As to the ripples, since their formation is related to the elastic strain relaxation, they were always found aligned along the two orthogonal [100] and [010] directions in the (001) oriented systems. If the observed interface undulations were due to ripples, they should be extended in three directions due to the threefold symmetry of our (111) oriented sample, which is not the case. Ripples can thus be excluded, too.

The orientation of the interface waviness in sample 2 indicates that it is strongly correlated with the steps. One may consider that the observed interface morphology is formed by a redistribution of the existing steps at the substrate surface when replicated into the epilayers. This way, the increased wave period means that more steps have been coalesced into a single bunch, leading to larger terraces as well as larger stepped facets. The nearly equal intensities of the diffuse peaks in the $-q_x$ and $+q_x$ regions in figure 5(a) suggest that the terraces and the stepped facets have similar face areas. In such an interface structure the steps are loosely bound. The wave period of 1.2 μm in sample 2 suggests a step-bunch size of about 39 and a mean step–step distance of about 15 nm in each bunch. This model is schematically shown in figure 3(b). The model shows interface waves with an amplitude (peak-to-valley height of the waves) of 6.2 nm. Considering that the amplitude of the surface waviness observed by AFM is about 6.4 ± 1.0 nm, the stress driven step redistribution shown in the proposed model is likely to be the dominant factor in the formation of the long-period interface waviness in sample 2.

The redistribution of the steps in the presence of misfit stress is thermodynamically favourable. When stress σ exists at the surface, the total free energy of a vicinal surface per unit area can be given by:

$$F_{total} = F^0(T) + \beta(T)n + \phi(T)/l^2 + \sigma^2 M \ln(l) \tag{1}$$

where F^0 is the surface energy of the terraces, β is the individual step free energy and they both are functions of surface temperature T. n represents the number of the steps. The third term in equation (1) corresponds to the repulsive step interaction energy arising from the 'force dipole' of the steps, and l is the step–step distance. The fourth term represents the attractive step interaction energy due to the epilayer strain, or a 'force monopole' [17, 25]. M is a system dependent parameter.

If the surface stress is so small that its contribution to F_{total} is negligible, the surface can be virtually treated as stress free. Since $F^0_{7\times7}(T < T_c) < F^0_{1\times1}(T < T_c)$, the Si(111) surface will be reconstructed below T_c to form flat 7×7 domains and densely stepped 1×1 domains [18, 27]. Consider a periodic arrangement of a 7×7 reconstructed terrace of width L separated by $(n-1)$ non-reconstructed terraces. The surface free energy, F, per unit area, can be expressed as

$$nlF = (nl - L)F^0_{1\times1} + LF^0_{7\times7} + n\beta + \phi/L^3 + (n-1)\phi/(nl-L)^3 \tag{2}$$

where l is the average step–step distance. The energy minimization condition $\mathrm{d}F/\mathrm{d}L = 0$ gives

$$F^0_{1\times1} - F^0_{7\times7} = 2\phi(n-1)^3/(nl-L)^3 - 2\phi/L^3. \tag{3}$$

Using the known values of $F_{1\times1} - F_{7\times7} = 2.1 \times 10^{-3}$ meV Å^{-2} and $\phi = 450$ meV Å [26, 27] and the measured bunch size $n = 12$ for sample 1, as well as the average step–step distance $l = 310$ Å determined from the miscut angle of 0.6°, we obtain $L = 2890$ Å. The unreconstructed domains are therefore $nl - L = 830$ Å wide. These results are in good agreement with those derived from the x-ray scattering data for sample 1.

When the stress σ becomes large enough, the fourth term in equation (1) plays an important role in the surface free energy. The consequence is that the original surface configuration, i.e., step bunching due to the reconstruction, becomes unstable towards step redistribution. By applying the energy minimization condition, $\mathrm{d}F/\mathrm{d}L = 0$, the equilibrium 7×7 terrace width could also be determined. However, because the stress induces a long-range step–step interaction, and the system parameter M is unknown, numerical analysis in this case is beyond the scope of this work. The step redistribution is governed by the net force, f, acting on the steps. For the mth step, the net force can be expressed as [17]

$$f_m = \sum_{m\neq n}\left(\frac{\sigma^2 A_1}{l_{mn}} - \frac{A_2}{l^3_{mn}}\right) \tag{4}$$

where A_1 and A_2 are system-dependent constants, l_{mn} is the distance between the mth and the nth steps. The first and the second terms in the summation are the attractive and repulsive forces between the mth and the nth steps, respectively. In principle, when the force balance is broken, step motion may happen. However, if σ is small, the velocity of this stress-driven step motion will be low, and the motion will probably be suppressed by a kinetic barrier due to depositing atoms and the limited growth temperature [17, 28]. This is most likely the case of our sample 1, in which the misfit strain is too small to cause a significant change in step configuration. The interface morphology of the multilayer is simply a replication of the substrate surface. If σ is large enough, e.g., in the alloy layers of sample 2, where the misfit strain (or the attractive force between steps) is three times (or almost one order of magnitude) larger than in sample 1, the net force acting on the steps can be large enough to overcome the kinetic barrier for step motion, leading to a step redistribution to minimize the surface free energy.

4. Concluding remarks

We have observed experimentally the dependence of interface morphology on the elastic strain in SiGe/Si multilayers grown on vicinal Si(111) substrates, by x-ray grazing-angle scattering. The interface morphology in the multilayer is unstable in the presence of misfit strain. If the misfit strain is small, the multilayer interfaces simply copy the morphology of the reconstructed Si(111) surface, showing closely bonded step bunches. On the other hand, if the strain is large, the surface steps will be redistributed, forming larger but looser step bunches. The driving force for the step redistribution is the surface free energy. Our AFM observation of the multilayer surfaces provides coherent pictures with the interface structures probed by the x-ray scattering method.

The present work provides an experimental support to stress-driven step bunching instability theoretically predicated by Tersoff and co-workers [17]. Though the instability is thermodynamic in origin, we found that the onset of this instability is subject to a kinetic barrier. Extended experimental investigations are needed to obtain a complete picture of the strain–interface morphology relationship. A means to this end is to grow a series of SiGe/Si multilayers with various Ge compositions on identical vicinal Si substrates, and to collect x-ray scattering data. A combined use of *in situ* scanning tunnelling microscopy (STM) will provide additional information, as demonstrated in this work.

Acknowledgments

We thank P M Reimer for useful discussions, and O Sakata for help in x-ray measurements. JHL would like to acknowledge JSPS for supporting his visit to Japan.

References

[1] Sinha S K, Garoff E B and Stanley H B 1988 *Phys. Rev.* B **38** 2297
[2] Savage D E, Kleiner J, Schimke N, Phang Y H, Jankowski T, Jacobs J, Kariotis R and Lagally M G 1991 *J. Appl. Phys.* **69** 1411
[3] Holy V, Kubena J, Ohlidal I, Lishika K and Plotz W 1993 *Phys. Rev.* B **47** 15 896
Holy V and Baumbach T 1994 *Phys. Rev.* B **49** 10 668
[4] Schlomka J P, Tolan M, Schwalowsky L, Seeck O H, Stettner J and Press W 1995 *Phys. Rev.* B **51** 2311
[5] Cullis A G 1996 *MRS Bull.* **21** 21–6
[6] Jesson D E, Chen K M and Pennycook S J 1996 *MRS Bull.* **21** 31–7
[7] Pidduck A J, Robbins D J, Cullis A G, Leong W Y and Pitt A M 1992 *Thin Solid Films* **222** 78
[8] For example, Usami N, Sunamura H, Fukatsu T and Shiraki Y 1995 *J. Cryst. Growth* **150** 1065
[9] Spencer B J, Voorhees P W and Davis S H 1991 *Phys. Rev. Lett.* **67** 3696
Spencer B J, Voorhees P W and Davis S H 1993 *J. Appl. Phys.* **73** 4955
[10] Xie Y H, Gilmer G H, Roland C, Silverman P J, Buratto S K, Cheng J Y, Fitzgerald E A, Kortan A R, Schuppler S, Marcus M A and Citrin P H 1995 *Phys. Rev. Lett.* **73** 3006
Tersoff J 1995 *Phys. Rev. Lett.* **74** 4962
[11] Dobbs H T and Vvedensky D D 1997 *Phys. Rev. Lett.* **79** 897
[12] Yu W and Madhukar A 1997 *Phys. Rev. Lett.* **79** 905
[13] Headrick R L and Baribeau J M 1993 *Phys. Rev.* B **48** 9174
Headrick R L, Baribeau J M and Strausser Y E 1995 *Appl. Phys. Lett.* **66** 96
[14] Phang Y H, Teichert C, Lagally M G, Peticolos L J, Bean J C and Kasper E 1994 *Phys. Rev.* B **50** 14 435
[15] Holy V, Giannini C, Tapfer L, Marschner T and Stolz W 1997 *Phys. Rev.* B **55** 9960
[16] Fitzgerald E A, Xie Y H, Monroe D, Silverman P J, Kuo J M, Kortan A R, Thiel F A and Weir B E 1992 *J. Vac. Sci. Technol.* B **10** 1807
[17] Tersoff J, Phang Y H, Zhang Z and Lagally M G 1995 *Phys. Rev. Lett.* **75** 2730
[18] Phaneuf R J, Williams E D and Bartelt N C 1988 *Phys. Rev.* B **38** 1984

[19] Fukatsu S, Usami N, Kato Y, Sunamura H, Shiraki Y, Oku H, Ohnish T, Ohmori Y and Okumura K 1994 *J. Cryst. Growth* **136** 355
[20] Reimer P M, Li J H, Yamaguchi Y, Sakata O, Hashizume H, Usami N and Shiraki Y 1997 *J. Phys.: Condens. Matter* **9** 4521
[21] Yoneda Y 1963 *Phys. Rev.* **131** 2010
[22] Noh D Y, Blum K I, Ramstad M J and Birgeneau R J 1993 *Phys. Rev.* B **48** 1612
[23] Held G A, Goodstein D M and Brock J D 1995 *Phys. Rev.* B **51** 7269
[24] Swartzentruber B S, Mo Y W, Webbs M B and Lagally M G 1989 *J. Vac. Sci. Technol.* A **7** 2901
[25] Alerhand O L, Vanderbilt D, Meade R D and Joannopoulos J D 1988 *Phys. Rev. Lett.* **61** 1973
[26] Hibino H and Ogino T 1994 *Phys. Rev. Lett.* **72** 657
[27] Willimas E D, Phaneuf R J, Wei J, Bartlet N C and Einstein T L 1993 *Surf. Sci.* **294** 219
[28] Kandel D and Weeks J D 1995 *Phys. Rev. Lett.* **74** 3632